

Accuracy of Proton T_1 Calculated by Approximations from Image Signals

Max S. Lin

Nuclear Medicine Service, V. A. Medical Center and Department of Internal Medicine, St. Louis University, St. Louis, Missouri

In proton magnetic resonance imaging, T_1 calculation from two measurements is simplified by using an approximation algorithm that assumes equilibrium recovery of longitudinal magnetizations or one that ignores refocusing 180° pulses used. Errors in calculated \hat{T}_1 arising from either approximation are evaluated using signal expressions that presume neither approximation. The approximation error depends on T_1 , sequence parameters, and the simplifying algorithm. The computed relation can be used to correct for the approximation error. The correction reduces calculated- \hat{T}_1 errors, but does not eliminate them, since other significant or potentially significant sources of the error are unaccounted for. These sources relate to ever-present stochastic noises, proper signal expressions, various instrumental factors, exponential compared with nonexponential nature of tissue proton relaxations, and tissue movements. The problem of quantitative T_1 measurement from image signals is briefly discussed.

J Nucl Med 26: 54-58, 1985

In proton magnetic resonance imaging, recognition of pathologic states relies primarily on image contrast, which varies with the radiofrequency (RF) pulse sequence used. Diagnostically optimal sequence in turn depends mainly on relaxation times of tissues to be differentiated (1-3). Knowledge of the relaxation properties acquired before or during a study facilitates the study in the initial imaging or in a reimaging in simulation or otherwise (3). A universally optimal sequence does not seem to exist.

Tissue T_1 can be calculated pixelwise from two image signals acquired with two pulse sequences of differing repetition times (4-7). Between the two sequences, the signal dependence on T_1 differs, but that on T_2 is identical. Two approximation algorithms have been used to simplify T_1 calculations yielding estimates of a qualitative utility. Equilibrium recovery of longitudinal magnetizations (M_z) in repetitive pulse cycles is assumed in one (4), and refocusing 180° pulses used are ignored treating spin-echo (SE) or double spin-echo (DSE) sequences as saturation recovery (SR) ones in the other (5). In this communication, calculated- T_1 errors arising

from one or the other approximation is evaluated using signal expressions that assume neither approximation.

SIGNAL EQUATIONS

Evaluation of algorithms for T_1 calculation begins with formulating full equations describing signals as functions of sequence and tissue parameters. For quantitative T_1 measurement as discussed later, proper signal equations depend on the imaging method and the extent of exponential character of tissue proton relaxations. Relatively simple functions suitable for computing signal values for varying sequence parameters and T_1 , but presuming neither of the approximations, were used in the present evaluation. For inversion recovery (IR), SE, or DSE sequences, these functions are given by

$$\text{IR: } S = 1 - 2e^{-T_1/T_1} + 2e^{-(T_R-1/2T_E)/T_1} - e^{-T_R/T_1} \quad (1)$$

$$\text{SE: } S = 1 - 2e^{-(T_R-1/2T_E)/T_1} + e^{-T_R/T_1} \quad (2)$$

$$\text{DSE: } S = 1 - 2e^{-(T_R-3/2T_E)/T_1} + 2e^{-(T_R-1/2T_E)/T_1} - e^{-T_R/T_1} \quad (3)$$

The pulse sequences are diagrammed in Fig. 1. For T_1 calculation, two measurements S_1 and S_2 are obtained using repetition times T_{R1} and T_{R2} , respectively, but an identical T_E delay. In DSE-DSE studies, both S_1 and S_2

Received Apr. 26, 1984; revision accepted Oct. 9, 1984.

For reprints contact: Max S. Lin, MD, PhD, Nuclear Medicine Service (115 JC), VA Medical Center, 915 N. Grand Blvd., St. Louis, MO 63106.

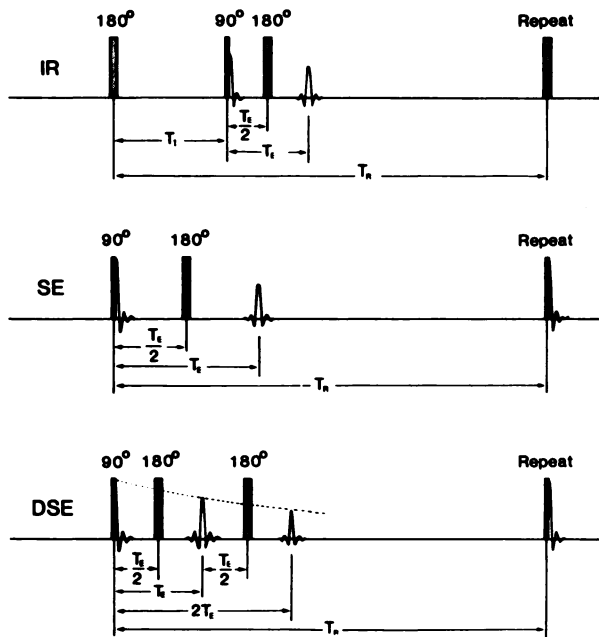


FIGURE 1
Schematic diagrams of inversion recovery (IR), spin-echo (SE), and double spin-echo (DSE) pulse sequences. Peaks of IR and SE echoes and first of two DSE echoes occur at time T_E from read 90° pulse and have amplitude e^{-T_E/T_2} relative to respective initial amplitudes at time zero. With IR sequence shown, data are gathered during spin echo as with SE sequence. Omitting refocusing 180° pulse from SE sequence turns sequence into SR one ($T_E = 0$)

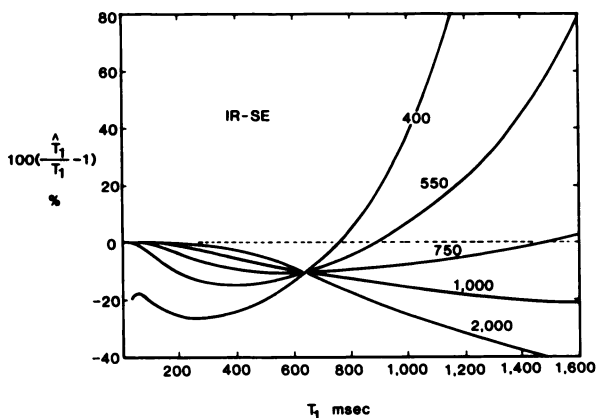


FIGURE 2
Fractional errors of \hat{T}_1 calculated by equilibrium approximation [(4)] for family of IR-SE studies with fixed IR sequence ($T_{R2} = 1700$ msec, $T_1 = 400$ msec), but varying SE sequence of varying T_{R1} (msec) as shown. Echo peaks at $T_E = 28$ msec in all sequences. Signals S_1 and S_2 of Eq. (4) are assumed to be given by Eqs. (2) and (1), respectively. Vertical ordering of five lines on short- T_1 side of intersection is exactly reverse of that shown for long- T_1 side

are based on the first echoes instead of the noisier second ones. In Eqs. (1)–(3), S describes S_1 for T_{R1} or S_2 for T_{R2} and has been normalized to the asymptotic signal for T_R much in excess of $5T_1$. The asymptote contains the signal

dependence on observable-proton density, tissue T_2 , and the echo delay T_E . The IR and SR signals in IR-SR studies are described by Eqs. (1) and (2), respectively, with T_E set to zero in the equations. In IR-SE studies, the IR and SE sequences (Fig. 1) may be combined into a composite one consisting of alternating IR and SE subsequences (7). The same is true of IR-SR studies.

EQUILIBRIUM APPROXIMATION

With IR signals represented by S_2 and SR ones by S_1 , the approximation states that T_1 is given by (4)

$$\hat{T}_1 = T_1 / \ln[2S_1 / (S_1 - S_2)]. \quad (4)$$

Equation (4) defines \hat{T}_1 , the measured or approximate T_1 . In other words, the approximation assumes that $T_1 = T_1 / \ln[2S_1 / (S_1 - S_2)]$, which is identical to

$$(S_2/S_1) - (1 - 2e^{-T_1/T_1}) = 0. \quad (5)$$

Eliminating $(1 - 2e^{-T_1/T_1})$ between (1) for $S_2(T_{R2})$ and (5), one has

$$(S_2/S_1)(1 - S_1) + 2e^{-(T_{R2}-1/2T_E)/T_1} - e^{-T_{R2}/T_1} = 0. \quad (6)$$

Upon eliminating $(1 - S_1)$ between (2) for $S_1(T_{R1})$ and (6), the assumption inherent in the approximation becomes

$$(S_2/S_1)[2e^{-(T_{R1}-1/2T_E)/T_1} - e^{-T_{R1}/T_1}] + 2e^{-(T_{R2}-1/2T_E)/T_1} - e^{-T_{R2}/T_1} = 0. \quad (7)$$

The assumption and the approximation are good when all exponential terms in (7) virtually vanish. This occurs with large T_{R1}/T_1 and T_{R2}/T_1 , that is, for spins of which T_1 is sufficiently shorter than T_{R1} and T_{R2} that their M_z virtually recovers to equilibrium values before the next cycle (6). To make the approximation good in this manner requires both T_{R1} and T_{R2} to exceed about $4T_1$ or $5T_1$ (7), quite feasible for the short- T_1 region of a usually broad T_1 band of clinical interest. For the most part of the band, the required $T_{R1} + T_{R2}$ time becomes impractically long.

Figures 2 and 3 show the fractional error of \hat{T}_1 for a family of IR-SE studies and a family of IR-SR studies, respectively. In both families, the IR sequence is fixed, and the other sequence is varied. In computing the approximation error, \hat{T}_1 is found according to Eq. (4) for S_1 and S_2 values calculated from Eqs. (2) and (1), respectively, for varying T_1 values. The fractional \hat{T}_1 error in percent is then plotted against T_1 . The \hat{T}_1 underestimates or overestimates T_1 to varying degrees depending on T_1 and sequence-parameter values (Figs. 2 and 3).

All lines of errors intersect at a point where the T_1 gives zero S_2 value by Eq. (1) and thus fixes the \hat{T}_1 at $T_1 / \ln 2$ by (4) regardless of S_1 or T_{R1} values (Figs. 2 and

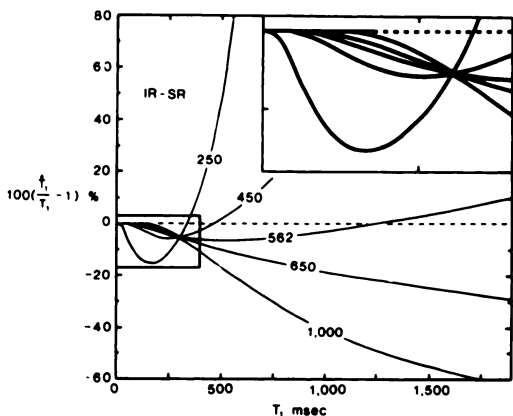


FIGURE 3

Fractional errors of \hat{T}_1 calculated by equilibrium approximation Eq. (4) for family of IR-SR studies with fixed IR sequence ($T_{R2} = 1000$ msec, $T_1 = 200$ msec), but varying SR sequence of varying T_{R1} (msec) as shown. Signal rephasing by gradient reversal is assumed in all sequences. S_1 and S_2 of Eq. (4) are based on Eqs. (2) and (1), respectively, for $T_E = 0$. Vertical ordering of five lines on the short- T_1 side of intersection is exactly reverse of that shown for long- T_1 side

3). The error line for T_{R1} 750 msec in Fig. 2 and that for T_{R1} 562 msec in Fig. 3 lie relatively close to the line of no error ($\hat{T}_1 = T_1$) over the entire T_1 range 100–1600 msec covering most normal and abnormal T_1 values at various imaging frequencies. Throughout this T_1 range, the absolute error is 10% or less for T_{R1} 750 msec in Fig. 2 and 6% or less for T_{R1} 562 msec in Fig. 3. Increasing T_{R1} to 2000 msec (Fig. 2) or 1000 msec (Fig. 3) better approximates equilibrium M_z recovery in the SE or SR sequence for all T_1 values. In so doing, however, the error for T_1 values shorter than the intersection T_1 (which is 305 msec in Fig. 3) decreases at best to zero, that for longer T_1 values increases substantially, and the overall approximation error across the said broad T_1 range increases considerably.

SATURATION RECOVERY APPROXIMATION

This approximation applies to imaging studies in which S_1 and S_2 are both SE, both DSE (5), or both multiple-echo (3) signals. The approximation is stated by (5)

$$S_1 = A(1 - e^{-T_{R1}/\hat{T}_1}) \quad (8)$$

$$S_2 = A(1 - e^{-T_{R2}/\hat{T}_1}). \quad (9)$$

Here, (8) and (9) define the measured or approximate T_1 . The asymptote A of the righthand-side quantities is normalized to the asymptote of S_1 and S_2 and cannot be less than unity.

Because of a disruption of M_z recovery by rephasing 180° pulses, SE and DSE signals are both smaller than SR ones for the same repetition time. In essence, the

approximation forces the SR expression $A(1 - e^{-T_R/\hat{T}_1})$ to describe S_1 or S_2 of less than SR size for no less proton abundance ($A \geq 1$). Consequently, the approximation systematically overestimates T_1 at all T_1 values. General expressions giving expected magnitudes of the overestimate can be derived for $T_{R2} = 2T_{R1}$ or $3T_{R1}$ (8):

$$\hat{T}_1 = T_{R1}/\ln[A/(A - S_1)], \quad (10)$$

$$\text{where, for } T_{R2} = 2T_{R1}, \quad A = S_1^2/(2S_1 - S_2), \quad (11)$$

for $T_{R2} = 3T_{R1}$,

$$A = [3S_1^2 + S_1(4S_1S_2 - 3S_2^2)^{1/2}]/2(3S_1 - S_2). \quad (12)$$

Figures 4 and 5 show the fractional error of the overestimate for T_{R2}/T_{R1} of 2 or 3. In computing the approximation error, S_1 and S_2 are calculated for varying T_1 values from Eq. (2) for SE-SE studies and from Eq. (3) for DSE-DSE studies and then used to compute \hat{T}_1 according to Eqs. (10) and (11) for $T_{R2} = 2T_{R1}$ or to Eqs. (10) and (12) for $T_{R2} = 3T_{R1}$. Results for the SE-SE studies (Fig. 4) and those for the DSE-DSE studies (Fig. 5) are nearly the same. The similarity stems from the fact that the T_1 dependence of DSE signals [(3)] is nearly identical in value to that of SE ones [(2)] for the same repetition time when the DSE second echo and the SE echo have the same delay. The shorter $T_{R1} + T_{R2}$ is for a given echo delay or the longer the delay is for a given $T_{R1} + T_{R2}$, the more inaccurate the approximation is (Figs. 4 and 5). For the same $T_{R1} + T_{R2}$ and delay, the accuracy is poorer at higher T_{R2}/T_{R1} , because SE- T_{R1} or DSE- T_{R1} mimics SR- T_{R1} poorly at small T_{R1}/T_1 . It is apparent that the approximation error can be substantial for relatively long T_1 at $T_{R1} + T_{R2}$ of 1500

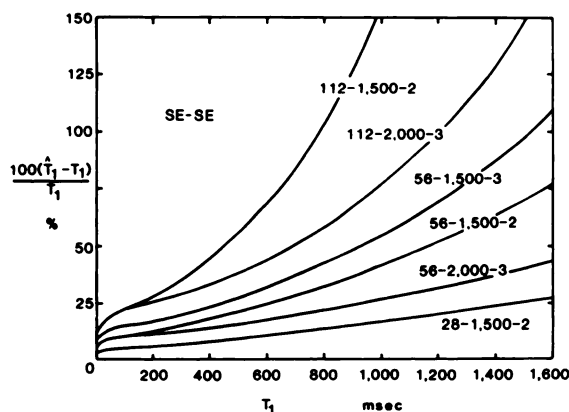


FIGURE 4

Fractional errors of \hat{T}_1 calculated by saturation recovery approximation for six SE-SE studies with varying echo time (T_E), sum of two repetition times ($T_{R1} + T_{R2}$), and their ratio (T_{R2}/T_{R1}). Notation "112-1500-2" signifies $T_E = 112$ msec, $T_{R1} + T_{R2} = 1500$ msec, and $T_{R2}/T_{R1} = 2$. Calculated error is based on \hat{T}_1 definition of Eqs. (8) and (9) and signal equation (2)

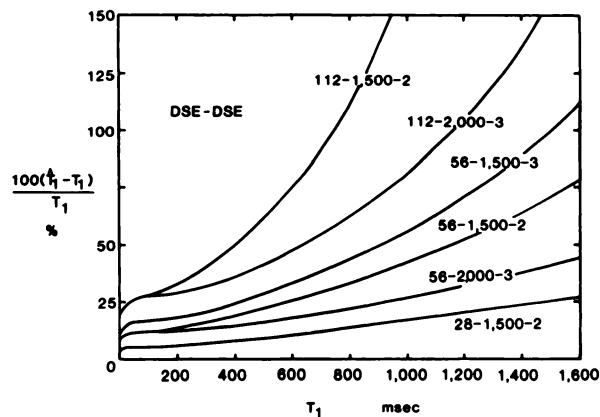


FIGURE 5

Fractional errors of \hat{T}_1 calculated by saturation recovery approximation for six DSE-DSE studies with varying echo time (T_E), sum of two repetition times ($T_{R1} + T_{R2}$), and their ratio (T_{R2}/T_{R1}). Notation "112-1500-2" denotes $2T_E = 112$ msec, $T_{R1} + T_{R2} = 1500$ msec, and $T_{R2}/T_{R1} = 2$. Calculated error is based on \hat{T}_1 definition of Eqs. (8) and (9) and signal equation (3)

msec and SE echo or DSE second-echo delay of 56 msec (Figs. 4 and 5).

DISCUSSION

Equations (1)–(3) or their virtual equivalents for zero or very short T_E values have been used to calculate T_1 (2,7,9) or image contrast (1,2) in the context of a planar imaging with selective 90° pulses (1,2,9) or a volumetric imaging with nonselective 90° (and 180°) pulses (1,7). The present \hat{T}_1 calculation is based on the assumption of Eqs. (1)–(3) and the simplifying definition of (4) or (8)–(9). With the SR approximation, the fractional \hat{T}_1 error increases with increasing T_1 faster than linearly (Figs. 4 and 5). Thus on a \hat{T}_1 map, the approximation would enhance or highlight abnormal T_1 , which is usually longer than the normal counterpart. The opposite is the case with equilibrium approximation using long T_{R1} . Here negative fractional errors decrease monotonously with increasing T_1 , and the extent of underestimation by \hat{T}_1 is greater for an abnormally lengthened T_1 than for the normal T_1 (Figs. 2 and 3). Nevertheless, such a calculated \hat{T}_1 in clinical studies serves a qualitative use (4).

A graph or table of T_1 compared with \hat{T}_1 can be used to correct calculated \hat{T}_1 from actual studies for said approximation errors. In DSE studies at 15 MHz using $T_{R1} + T_{R2} = 1500$ msec, $T_{R2}/T_{R1} = 2$, and $2T_E = 56$ msec, for example, \hat{T}_1 of dilute (postcholecystogogue) gallbladder bile was reported to average 2324 msec by SR approximation in six normal volunteers, the longest of the six values being 3152 msec (10). Corrected on the basis of Eq. (3), the 3152-msec \hat{T}_1 shortens to 1697 msec, a value reasonably close to the T_1 estimate of 1700–1750

msec for the free-water component of tissue water (11).

The correction reduces errors in the calculated \hat{T}_1 , but does not eliminate them. Signals acquired in actual studies are adulterated by random noises. Effect of blood flow and physiologic motion, if any, is not accounted for in Eqs. (1)–(3) either. From the standpoint of imaging method, Eqs. (1)–(3) are proper with nonselective excitation using broadband 90° (and 180°) pulses as in a few volumetric imaging techniques (7,12,13). The validity can suffer from various instrumental factors such as wrong settings of pulse angles and nonuniform RF fields. In particular, total decay of signals (or transverse magnetizations) within individual cycles with no regrowth in subsequent cycles is assumed in Eqs. (1)–(3) (7,8). "Spoiler gradients" applied to achieve the condition of zero residual signals must and can work properly (7,8,14).

With planar imaging using selective 90° pulses, single slice or multislice, propriety of Eqs. (1)–(3) requires the slice profile to be essentially rectangular as can be met when the 90° pulse is modulated with an envelope having the form of a sinc function (14). Summation of signal contributions over a substantially nonrectangular slice profile can yield signal expressions containing integrals that are laborious to evaluate (15). In a nonrectangular case, Eqs. (1)–(3) are approximations good to the extent that the profile peak (center-plane signal) and the profile area (total signal) are related by a constant factor or experimentally to the extent that predictions based on simple equations agree with actually acquired images (2,3).

Equations (1)–(3) further assume a single T_1 for a pixel volume. A potential problem with this presumption is that many proton spin systems of different relaxation properties exist in a typical voxel. For nonadipose tissues, however, image signals should derive primarily from water protons (16), signals from organic protons being of small abundance or due to very short T_2 being largely lost in the time to rephase the signal for detection (17,18). In spectroscopic studies in vitro, the transverse relaxation of water protons in skeletal muscles is virtually, though not exactly, exponential for about the first 150–200 msec (19), and the longitudinal relaxation in most tissues is characterized to a good approximation by a single T_1 (20). In a fast exchange in theory, a rapid water turnover relative to its relaxation in each region within a voxel can result in essentially a single observable T_1 or T_2 for the voxel water protons as a whole (16).

Another problem with quantitative T_1 measurement in vivo relates to partial-volume effect especially where major tissue elements within a voxel differ grossly in their relaxation parameters and undergo no or slow exchange of their visible protons. A weighted average T_1 for the voxel should vary to a degree with varying T_2 and relative abundance among the elements and with se-

quence parameters, all of which can affect the weighting. Adipose triacylglycerol protons appear to have T_1 values substantially shorter than those of water protons of most other soft tissues (17,21). Adipose tissues, which are about 80% triacylglycerols by weight (22), and loose connective tissues rich in adipocytes are ubiquitous. In anatomical regions where the lipid and water protons codominate visible protons, it is quite possible for calculated T_1 pixelwise or averaged over multiple pixels to depend appreciably on sequence parameters used. Such partial-volume problems can be reduced by going to a high-resolution imaging subject to the constraint of available imaging time and signal-to-noise (S/N) consideration in relation to stochastic observable- T_1 uncertainty. The S values of Eqs. (1)–(3) are in units of the asymptote $S(\infty)$, which is proportional to e^{-T_E/T_2} . At a given noise level, larger T_E/T_2 values give lower S/N and higher stochastic T_1 uncertainty.

ACKNOWLEDGMENT

The author gratefully acknowledges encouragement of Robert M. Donati, M.D., Senior Associate Dean, St. Louis University School of Medicine.

REFERENCES

- Hart HR Jr, Bottomley PA, Edelstein WA, et al: Nuclear magnetic resonance imaging: Contrast-to-noise ratio as a function of strength of magnetic field. *Am J Roentgenol* 141:1195–1201, 1983
- Wehrli FW, MacFall JR, Shutts D, et al: Mechanisms of contrast in NMR imaging. *J Comput Assist Tomogr* 8:369–380, 1984
- Bielke G, Meves M, Meindl S, et al: A systematic approach to optimization of pulse sequences in NMR imaging by computer simulations. In *Technology of Nuclear Magnetic Resonance*, Esser PD, Johnston RE, eds. New York, The Society of Nuclear Medicine, 1984, pp 109–117
- Hutchison JMS, Smith FW: NMR clinical results: Aberdeen. In *Nuclear Magnetic Resonance (NMR) Imaging*, Partain CL, James AE, Rollo FD, et al, eds. Philadelphia, W. B. Saunders, 1983, pp 231–249
- Herfkens R, Davis P, Crooks L, et al: Nuclear magnetic resonance imaging of the abnormal live rat and correlations with tissue characteristics. *Radiology* 141:211–218, 1981
- Redpath TW: Calibration of the Aberdeen NMR imager for proton spin-lattice relaxation time measurement *in vivo*. *Phys Med Biol* 27:1057–1065, 1982
- Pykett IL, Rosen BR, Buonanno FS, et al: Measurement of spin-lattice relaxation times in nuclear magnetic resonance imaging. *Phys Med Biol* 28:723–729, 1983
- Lin MS: Measurement of spin-lattice relaxation times in double spin-echo imaging. *Magn Reson Med* 1:361–369, 1984
- Gore JC, Doyle FH, Pennock JM: Relaxation rate enhancement observed *in vivo* by NMR imaging. In *Nuclear Magnetic Resonance (NMR) Imaging*, Partain CL, James AE Jr, Rollo FD, et al., eds. Philadelphia, W. B. Saunders, 1983, pp 94–106
- Hricak H, Filly RA, Margulis AR, et al: Work in progress: Nuclear magnetic resonance imaging of the gallbladder. *Radiology* 147:481–484, 1983
- Escanye JM, Canet D, Robert J: Frequency dependence of water proton longitudinal nuclear magnetic relaxation times in mouse tissues at 20°C. *BBA* 721:305–311, 1982
- Pykett IL, Buonanno FS, Brady TJ, et al: True three-dimensional nuclear magnetic resonance neuro-imaging in ischemic stroke: Correlation of NMR, X-ray CT and pathology. *Stroke* 14:173–177, 1983
- Hutchison JMS: NMR scanning: The spin warp method. In *NMR Imaging*; Witcofski RL, Karstaedt N, Partain CL, eds. Winston-Salem, The Bowman Gray School of Medicine, 1982, pp 77–80
- Edelstein WA, Bottomley PA, Hart HR Jr, et al: Signal, noise, and contrast in nuclear magnetic resonance (NMR) imaging. *J Comput Assist Tomogr* 7:391–401, 1983
- Rosen BR, Pykett IL, Brady TJ: Spin lattice relaxation time measurements in two-dimensional nuclear magnetic resonance imaging: Corrections for plane selection and pulse sequence. *J Comput Assist Tomogr* 8:195–199, 1984
- Mathur-De Vré R: The NMR studies of water in biological systems. *Prog Biophys Mol Biol* 35:103–134, 1978
- Inch WR, McCredie JA, Knispel RR, et al: Water content and proton spin relaxation time for neoplastic and non-neoplastic tissues from mice and humans. *J Natl Cancer Inst* 52:353–356, 1974
- Fung BM: Carbon-13 and proton magnetic resonance of mouse muscle. *Biophys J* 19:315–319, 1977
- Fung BM, Puon PS: Nuclear magnetic resonance transverse relaxation in muscle water. *Biophys J* 33:27–37, 1981
- Ling CR, Foster MA, Hutchison JMS: Comparison of NMR water proton T_1 relaxation times of rabbit tissues at 24 MHz and 2.5 MHz. *Phys Med Biol* 25:748–751, 1980
- Shaw D: *In vivo* topical magnetic resonance. In *Nuclear Magnetic Resonance (NMR) Imaging*, Partain CL, James AE Jr, Rollo FD, et al., eds. Philadelphia, W. B. Saunders, 1983, pp 152–167
- Morse WI, Soeldner JS: The measurement of human adipose tissue mass. In *Handbook of Physiology, Section 5: Adipose Tissue*, Renold AE, Cahill GE Jr, eds. Washington, D.C., The American Physiological Society, 1965, pp 653–659